Journal of Geophysical Research: Atmospheres

RESEARCH ARTICLE
10.1029/2018JD029321

**Key Points:**
- The seasonal evolution of stratosphere-troposphere coupling in the Southern Hemisphere (SH) is explored and updated using height-time domain EOF analysis
- Variability in the SH tropospheric annular mode in spring-summer is significantly linked to the extratropical vortex as high as the stratopause and as early as June

**Supporting Information:**
- Supporting Information S1

**Correspondence to:**
E.-P. Lim,
e.lim@bom.gov.au

**Citation:**
Lim, E.-P., Hendon, H. H., & Thompson, D. W. J. (2018). On the seasonal evolution and impacts of stratosphere-troposphere coupling in the Southern Hemisphere. *Journal of Geophysical Research: Atmospheres*, *123*, 12,002–12,016. https://doi.org/10.1029/2018JD029321

Received 12 JUL 2018
Accepted 17 OCT 2018
Accepted article online 22 OCT 2018
Published online 10 NOV 2018



# Seasonal Evolution of Stratosphere-Troposphere Coupling in the Southern Hemisphere and Implications for the Predictability of Surface Climate

**E.-P. Lim[1], H. H. Hendon[1], and D. W. J. Thompson[2]**

[1]Bureau of Meteorology, Melbourne, Victoria, Australia, [2]Department of Atmospheric Science, Colorado State University, Fort Collins, CO, USA

**Abstract** Stratosphere-troposphere coupling in the Southern Hemisphere (SH) polar vortex is an important dynamical process that provides predictability of the tropospheric Southern Annular Mode (SAM) and its associated surface impacts. SH stratosphere-troposphere coupling is explored by height-time domain empirical orthogonal function (EOF) analysis applied to the zonal mean-zonal wind anomalies averaged over the Antarctic circumpolar region (55–65°S; $U_{55-65°S}$). The leading EOF explains 42% of the height-time variance of $U_{55-65°S}$ and depicts the variations of the vortex that is tightly tied to the seasonal breakdown of the vortex during late spring. The leading EOF pattern, defined here as the stratosphere-troposphere coupled mode, is characterized by variations in $U_{55-65°S}$ that develop in early winter near the stratopause, change sign from late winter to early spring, gain maximum amplitude during October in the upper stratosphere, and then extend downward to the surface from October to January. This stratosphere-troposphere coupling during the spring months appears to be preconditioned by anomalies in upward propagating planetary wave activity and a meridional shift of the vortex as high as the stratopause and as early as June. Interannual variations of the stratosphere-troposphere coupled mode are highly correlated with those of the tropospheric SAM, Antarctic stratospheric ozone concentration, Antarctic sea ice concentrations in the South Pacific and the Weddell Sea, and SH regional climate during late spring–early summer. Anomalies in the upper stratospheric flow as early as June are thus a potentially important source of predictability for the tropospheric SAM and its associated impacts on surface climate in spring and summer.

**Plain Language Summary** We have explored the seasonal evolution of the strength of the Southern Hemisphere (SH) stratospheric polar vortex and its coupling to the lower atmosphere in 1979–2017, using atmospheric reanalyses that assimilate observational data. Variations in the strength of the Antarctic circumpolar flow in the troposphere during austral late spring to early summer are found to be coupled to variations in position and strength of the stratospheric vortex as high as the stratopause and as early as the preceding June, notably higher and earlier than indicated in previous studies. This suggests that variations in the winter upper stratospheric jet can serve as a potentially important source of predictability for SH surface climate in the late spring–early summer. We explore the physical processes associated with the seasonal evolution of SH stratosphere-troposphere coupling and its impacts on surface climate.

## 1. Introduction

Downward coupling of variability in the polar stratosphere drives low frequency variations in tropospheric circulation and temperature and thus can serve as a source of extended range predictability of surface weather and climate (e.g., Baldwin et al., 2003; Baldwin & Dunkerton, 2001; Charlton et al., 2003; Roff et al., 2011; Sigmond et al., 2013). The most dramatic examples of downward coupling occur in association with sudden stratospheric warmings (SSWs), which commonly occur in the Northern Hemisphere (NH) in early winter to early spring season. SSWs are instigated by anomalously increased planetary wave activity propagating upward from the troposphere in middle to high latitudes and are manifested by weakening of the stratospheric westerly jet and rapid warming of the polar stratosphere within a few days to a week (e.g., Butler et al., 2015, and references therein). These stratospheric changes sometimes propagate downward and affect the surface climate via promoting the negative phase of the North Atlantic Oscillation/Northern Annular Mode that can last up to 1–2 months, therefore causing potentially predictable anomalous weather conditions over the North Atlantic rim countries (e.g., Baldwin et al., 2003; Baldwin & Dunkerton, 1999; Butler

et al., 2015; Kidston et al., 2015; Sigmond et al., 2013) and the North Atlantic ocean (e.g., Menary & Scaife, 2014; Reichler et al., 2012). The opposite phenomenon is described as polar vortex intensification whose development, downward coupling, and recovery occur more gradually than those of SSWs (Limpasuvan et al., 2005) but similarly can result in long-lived swings to the positive phase of the North Atlantic Oscillation/Northern Annular Mode.

Polar vortex variations also occur in the Southern Hemisphere (SH) stratosphere but are generally weaker than those in the NH due to weaker planetary wave activity in the SH (Graversen & Christiansen, 2003; Shiotani & Hirota, 1985; Taguchi & Yoden, 2002). Polar vortex variability is strongly tied to the seasonal cycle, and in the SH the variability peaks in austral spring when the speed of the stratospheric polar night jet seasonally weakens so as to be susceptible to forcing by planetary waves propagating upward from the troposphere (e.g., Kuroda & Kodera, 1998; Randel, 1988; Shiotani & Hirota, 1985; Thompson & Wallace, 2000). SH stratospheric polar vortex weakening and intensification can lead to the negative (−ve) and positive (+ve) phases of the tropospheric Southern Annular Mode (SAM; hereafter, SAM denotes the tropospheric component of the SAM unless otherwise stated), respectively, in spring (Baldwin et al., 2003; Byrne & Shepherd, 2018; Thompson et al., 2005).

The SAM is the dominant mode of variability of SH extratropical tropospheric circulation at timescales longer than a couple of weeks (e.g., Hartmann & Lo, 1998; Karoly, 1990; Kidson, 1988; Thompson & Wallace, 2000), and it impacts surface climate throughout the subtropics, extratropics, and polar regions of the SH on timescales from days to seasons (e.g., Arblaster et al., 2014; Gillett et al., 2006; Gupta & England, 2006; Hall & Visbeck, 2002; Hendon et al., 2007, 2014; Kang et al., 2011; Lefebvre et al., 2004; Lim et al., 2016; Lim & Hendon, 2015a; Marshall et al., 2017; Reason & Rouault, 2005; Silvestri & Vera, 2003; Thompson & Solomon, 2002). Hence, stratosphere-troposphere (S-T) coupling is a potential source of extended range predictability for SH climate much as it is for the NH (e.g., Baldwin et al., 2003; Byrne & Shepherd, 2018; Roff et al., 2011; Seviour et al., 2014).

This study builds on earlier research that has also explored the nature of stratospheric vortex variability and S-T coupling in the SH (e.g., Byrne & Shepherd, 2018; Kuroda & Kodera, 1998; Randel, 1988; Shiotani & Hirota, 1985; Thompson et al., 2005; Thompson & Wallace, 2000). Especially, we focus on precursor signals in the uppermost stratosphere as high at 1 hPa and throughout the SH winter months. A key novel result is that SH surface climate anomalies during the spring months can be traced back to the state of the vortex near the stratopause level in June, which is both higher and earlier than the linkages indicated in previous work (e.g., Byrne & Shepherd, 2018; Seviour et al., 2014).

In order to capture the height-time evolution of vortex variability that is tightly tied to the seasonal breakdown of the vortex, we use height-time domain empirical orthogonal function (EOF) analysis (e.g., North et al., 1982), which was referred to as multiple EOF in Kuroda and Kodera (1998), Taguchi and Yoden (2002), and Hio and Yoden (2005). The observationally based data sets and the height-time domain EOF method are described in section 2. The dynamics and impacts of the leading mode of variability that emerges from height-time EOF analysis of the SH polar flow are explored in sections 3 and 4, respectively. Concluding remarks are presented in section 5.

## 2. The SH *Stratosphere-Troposphere Coupled Mode*

We use ERA-Interim (ECMWF re-analysis-Interim) monthly mean reanalyses for atmospheric variables for 1979 January to 2017 March (Dee et al., 2011). Pressure level data are available at 37 levels from 1 to 1,000 hPa with 1.5° spatial resolution. We also use ERA-Interim instantaneous daily zonal and meridional wind and temperature fields at 00Z to diagnose the anomalous eddy fluxes of momentum and heat.

The leading pattern of seasonally and vertically varying variability in the SH high latitude atmosphere is revealed using height-time domain EOF analysis (covariance matrix), which was referred to as multiple EOF analysis in earlier studies (Hio & Yoden, 2005; Kuroda & Kodera, 1998; Taguchi & Yoden, 2002). To conduct this EOF analysis, we first compute area-averaged zonal mean-zonal wind anomalies over the latitude band 55–65°S ($U_{55-65°S}$). Anomalies are computed as departures from the monthly mean climatology averaged over 1979–2016. The latitude band 55–65°S was chosen because zonal mean-zonal wind variations there capture variability in both the stratospheric polar night jet and the tropospheric component of the SAM (e.g., Kuroda & Kodera, 1998). To prepare the data for input into the EOF analysis, $U_{55-65°S}$ was formed as a function of pressure level ($l$) and calendar month ($t$) for each year ($y$), so that the shape of the

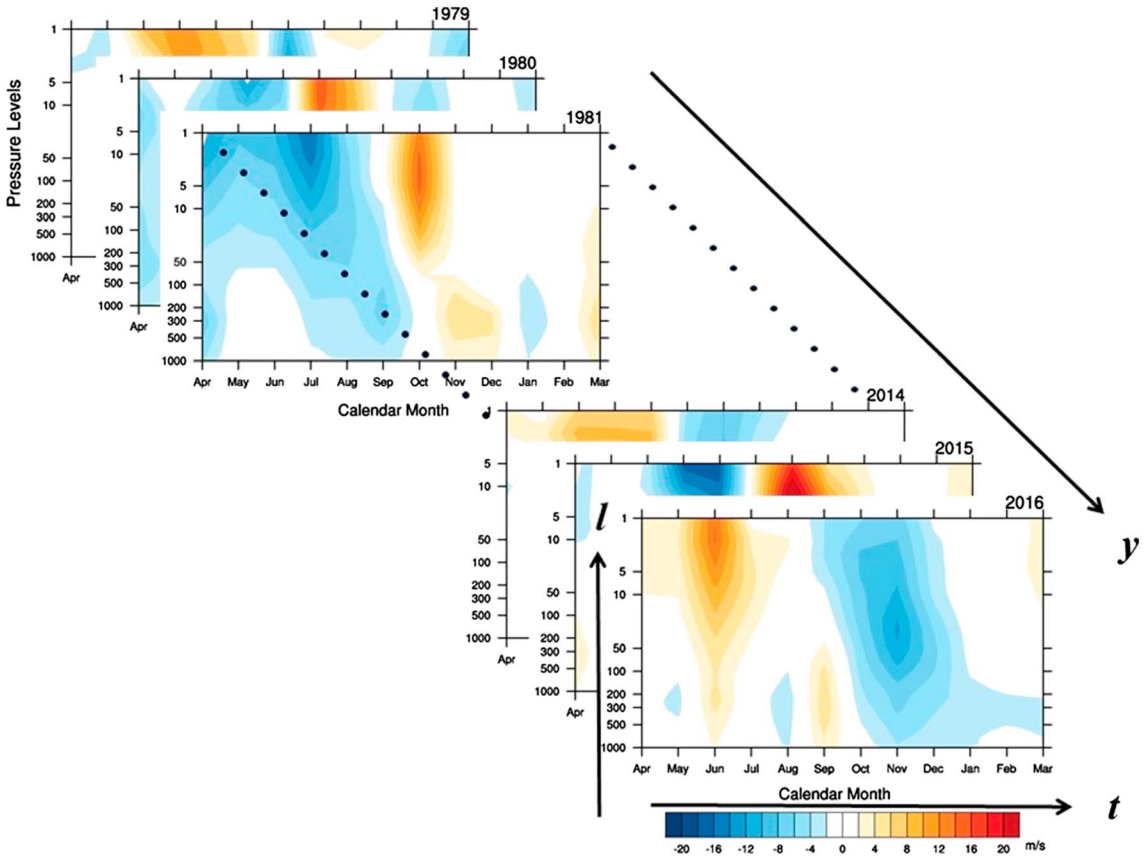


**Figure 1.** Illustration of the data preparation as a function of pressure level (*l*), calendar month (*t*), and year (*y*) before the empirical orthogonal function (EOF) analysis. Real data are used for the illustration. The calendar months run from April to March to encompass austral spring and summer months when active stratosphere-troposphere downward coupling occurs.

input data matrix *X* to the EOF analysis is (**S**, Y). Here **S** is 37 vertical levels for 12 calendar months, and Y is 38 years. A schematic of the input data matrix is displayed in Figure 1. The calendar months for each year are specified to run from April to the following year's March to make the data continuous across the spring-summer season when the vortex is the most variable (e.g., Black & McDaniel, 2007; Hartmann et al., 1984; Kuroda & Kodera, 1998; Shiotani et al., 1993). Note that Byrne and Shepherd (2018) recently applied a similar multiple EOF analysis to also explore seasonally phase-locked vortex variability, but they only used winds at one vertical level.

The outputs of the height-time domain EOF analysis are an eigenvector *E* that is a function of vertical level and calendar month (from April to March) and its expansion coefficient or principal component *p* that is a function of year. The input data *X* can then be reconstructed as

$$X(l,t,y) = \Sigma_{m=1}^{M} E(l,t)_m p(y)_m,$$

where *l* indicates pressure levels (1 to 37), *t* is calendar month (1 to 12) that runs from April to March each year, and *y* is year (1 to 38). *M* (=37 × 12) denotes the number of eigenmodes.

The height-time domain EOF used here isolates variability that has common seasonal evolution from one year to the next. This approach is justified by examination of the interannual variance of the input data *X* calculated as a function of calendar month (shading in Figure 2). Maximum variance of the Antarctic circumpolar circulation is strongly tied to the seasonal cycle, peaking near the stratopause in winter and in the upper stratosphere in spring and then extending downward to the troposphere in spring-summer in conjunction with seasonal weakening of the polar night jet (e.g., Kodera & Kuroda, 2002; Shiotani et al., 1993; Thompson et al., 2005; Thompson & Wallace, 2000). The EOF analysis will return

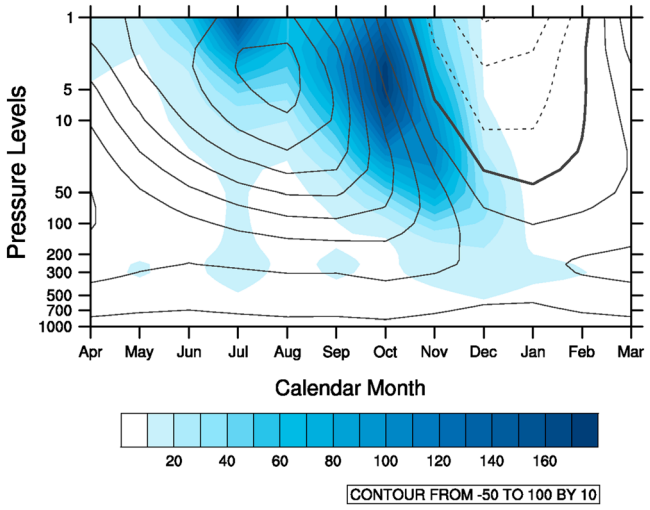


**Figure 2.** Climatology (contours) and interannual variance (shading) of the monthly mean zonal mean-zonal winds averaged over 55–65°S using ERA-Interim reanalysis for the period 1979 April to 2017 March. Negative contours are dashed, and the zero contour is thickened.

the leading pattern of variability in the height/calendar month domain that captures the vertical-temporal evolution of the polar vortex that is tightly tied to the seasonal cycle.

The leading EOF and its associated principal component (PC) time series (Figures 3a and 3b; also supporting information Figure S1) explain 42% of the total variance of the Antarctic circumpolar flow in the height/calendar month domain. The EOF is dominated by variability in the circumpolar flow in the stratosphere in late winter to spring that extends downward to the troposphere in mid-spring to early summer, being consistent with the seasonal variation in the variance of the Antarctic circumpolar wind (Figure 2). Hereafter, we will call this pattern the SH S-T coupled mode. We define positive values of the principal component time series (PC1; also referred to as the S-T coupled mode index) as periods of easterly anomalies or weakening of the springtime polar vortex. Note that the polarity of the S-T coupled mode is defined such that its positive polarity projects onto the negative polarity of the SAM (-ve SAM) during the spring-summer months. The corresponding evolution of polar cap geopotential height and temperature is found by regressing the respective fields onto the PC1 time series (Figures 3c and 3d). As expected, the weakening of the stratospheric polar vortex is accompanied by increases in geopotential height and temperature over the Antarctic polar cap. The polar cap warming is driven predominantly by anomalous (residual) downward motion (e.g., McIntyre, 1982) but also partially by higher concentrations of stratospheric ozone resulting from the weakening of the polar vortex (e.g., Stolarski et al., 2005).

The interannual variability of the S-T coupled mode represented by PC1 (Figure 3a) indicates that 2002 had the most extreme vortex weakening within the period of available data (e.g., refer to the special issue of Journal of the Atmospheric Science on the Antarctic stratospheric sudden warming and split ozone hole of 2002 [2005, Vol.62, No. 3]; Butler et al., 2015; Dowdy et al., 2007). This event resulted in near record reduction of the Antarctic ozone hole and record strong −ve SAM during austral spring (Dowdy et al., 2007; Hio & Yoden, 2005; Lim & Hendon, 2015b; Newman & Nash, 2005; Thompson et al., 2005). The strong −ve SAM contributed to the devastating drought over Australia (Lim & Hendon, 2015b) and to heavy rainfall over southern Chile (World Meteorological Organization, 2003). Significant vortex weakening with smaller amplitudes than the 2002 event (PC1 $\geq$ 0.8 standard deviation [$\sigma$]) also occurred in 1979, 1988, 2000, 2004, 2005, 2012, 2013, and 2016. The strongest polar vortex intensification event (PC1 $\leq -0.8\sigma$) is found in 1987 closely followed by 2015, and 1995, 1998, 1999, 2001, 2006, 2010, and 2011. Many of the polar vortex weakening and strengthening events picked by our method well match those listed in Thompson et al. (2005) and those displayed in Hio and Yoden (2005) and Byrne and Shepherd (2018).

One may question if interannual variability of the S-T coupled mode is linked to variations in the El Niño–Southern Oscillation (ENSO). ENSO is significantly linked to the SAM during spring-summer: The negative polarity of the tropospheric SAM tends to occur during the warm phase of the ENSO cycle, and its positive polarity tends to occur during the cold phase of the ENSO cycle (e.g., Seager et al., 2003; L'Heureux & Thompson, 2006; Lim et al., 2013). Regarding the SH polar vortex variability, Hurwitz et al. (2011, 2014) showed that central equatorial Pacific sea surface temperature (SST) variations could be linked to changes in planetary wave activity in the Antarctic polar vortex in November to December. Byrne et al. (2017) also reported a tendency of more frequent occurrence of early vortex breakdown during warm years of the ENSO cycle and the opposite tendency during cold years. However, the correlation between the S-T coupled mode PC1 and eastern Pacific SST is not statistically significant, and the correlation with central Pacific SST is only marginally significant (supporting information Figure S2). Because variability of the S-T coupled mode is not strongly related to ENSO, there are times when the S-T coupled mode and ENSO act together to increase the amplitude of the SAM (e.g., the concurrence of the warm phase of ENSO and weak vortex events during 2002 and 2004/the cold phase of ENSO and strong vortex events during 1998, 1999, and 2010) and times

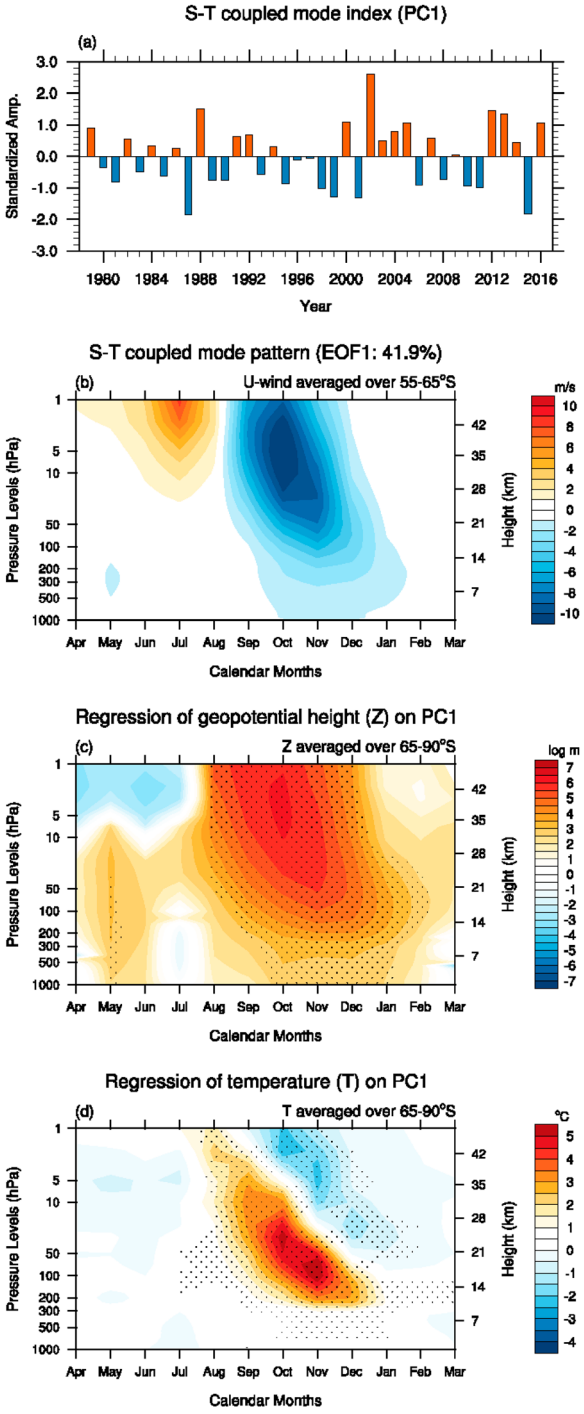


**Figure 3.** The stratosphere-troposphere (S-T) coupled mode captured by the first mode of height-time domain EOF analysis applied to the monthly mean zonal mean-zonal wind anomalies averaged over the latitude band of 55–65°S. (a) The S-T coupled mode principal component time series (PC1), (b) the S-T coupled mode eigenvector (EOF1), (c) regression of geopotential height anomalies averaged 65–90°S onto PC1, and (d) same as (c) except for temperature anomalies averaged 65–90°S. Regression coefficients for geopotential height anomalies in (c) are plotted using a log scale. The positive phase of the S-T coupled mode represents weakening of the spring polar vortex. Stippling in (c) and (d) indicates statistical significance of regression coefficients at the 5% level, assessed by a two-tailed Student *t* test with 38 samples. The S-T coupled mode PC1 and its pattern displayed in (a) and (b) are not dependent on a particular data set used here as PC1 and EOF1 produced using the Japanese 55-year Reanalysis (Kobayashi et al., 2015) are almost identical to (a) and (b). The structure of the S-T coupled mode pattern is maintained in the longer record of Japanese 55-year Reanalysis starting from 1958 (see supporting information Figure S1).

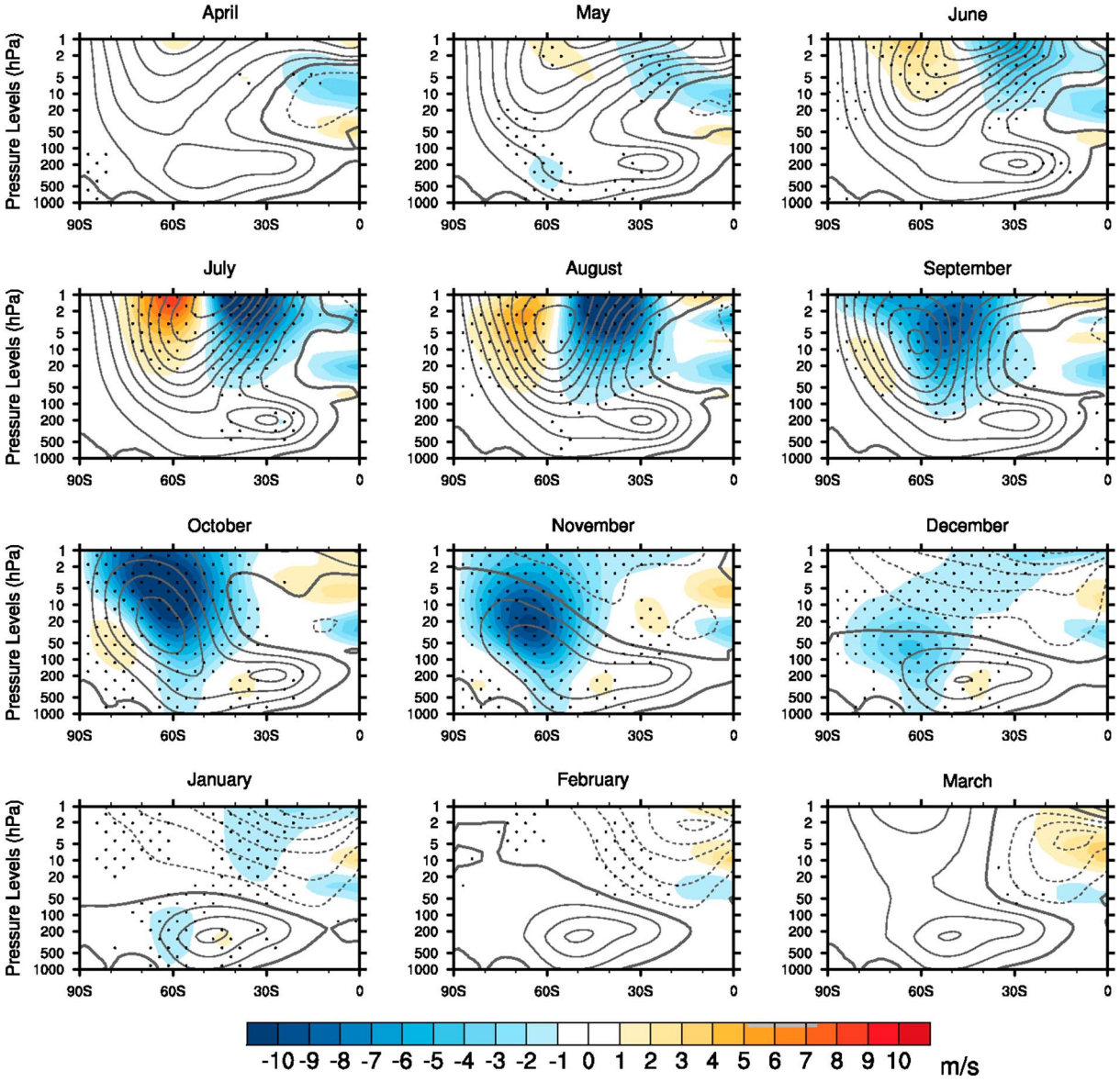


**Figure 4.** Regression of monthly anomalies of zonal mean-zonal wind onto PC1 (shading; interval is 1 m/s). The monthly climatology of zonal mean-zonal winds is contoured (interval is10 m/s; zero contour is thick, and negative contours are dashed). Stippling indicates statistical significance of regression coefficients at the 5% level, assessed by a two-tailed Student *t* test with 38 samples.

when they oppose each other's influence on the SAM (e.g., the concurrence of the warm phase of ENSO and strong vortex events during 1987, 2006, and 2015/the cold phase of ENSO and weak vortex events during 1988 and 2016). More detailed analyses of the linkages between the S-T coupled mode and tropical Pacific SSTs are beyond the scope of this study.

Vortex weakening events (i.e., positive values of PC1) appear to have increased post-2000, consistent with Figure 4 in Byrne and Shepherd (2018), which may be associated with recovery of the Antarctic ozone hole (e.g., Solomon et al., 2016). However, PC1 does not exhibit a significant trend over the period 1979 to early 2017 in contrast to the significant positive trend in the SAM over this period (e.g., Thompson & Solomon, 2002) and the delay in the timing of the final stratospheric warming (e.g., Black & McDaniel, 2007; Hirano et al., 2016; Waugh et al., 1999), both of which have been attributed to the stratospheric ozone depletion.

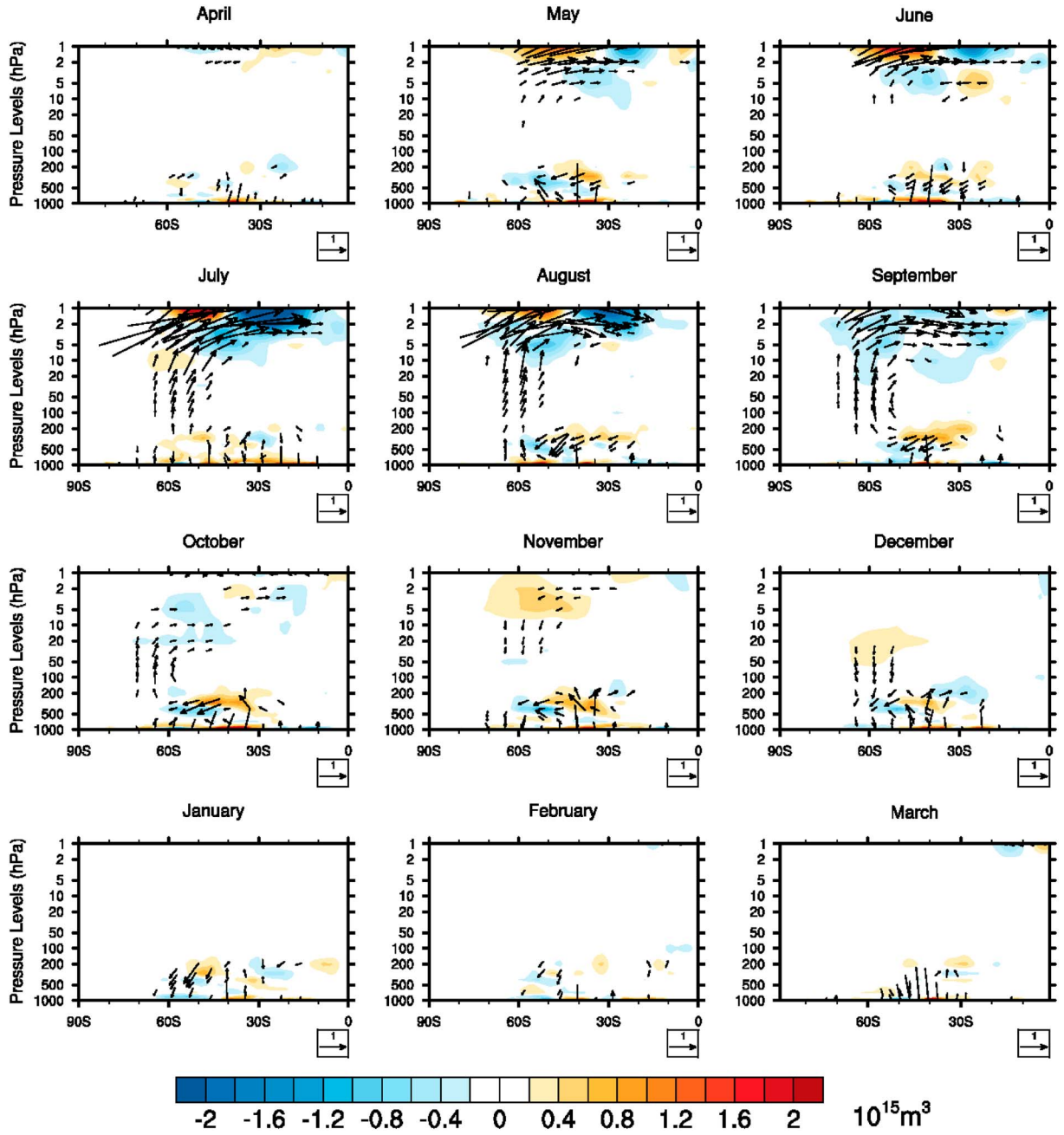


**Figure 5.** Regression of anomalies of E-P flux (vectors; vector scale in lower right) and E-P flux divergence (shading; interval is $0.2 \times 10^{15}$ $m^3$) onto PC1. E-P flux and divergence calculations follow Peixoto and Oort (1992). The vector scale unit is $10^{15}$ $m^3$ in horizontal direction and $10^{17}$ $m^3$·kPa in vertical direction. The E-P flux vectors were scaled by the inverse square root of pressure, taking 100 hPa as a reference first and then scaled by 2 below the 10-hPa level for improved visibility of vectors. Vectors with magnitudes less than 0.2 are not displayed.

## 3. Dynamical Evolution of the S-T Coupled Mode and Its Linkage With the SAM

### 3.1. Life Cycle of the S-T Coupled Mode

The latitude-height evolution of the S-T coupled mode through the seasonal cycle is explored further by regressing monthly mean zonal mean-zonal wind anomalies onto PC1 (Figure 4). Here we describe the evolution associated with the positive index polarity of PC1. For reference, the climatological zonal mean-zonal wind is overlain (contours). The climatological mean stratospheric westerly jet starts to develop through autumn with the stratopause jet core moving equatorward (Kodera & Kuroda, 2002). The jet strengthens

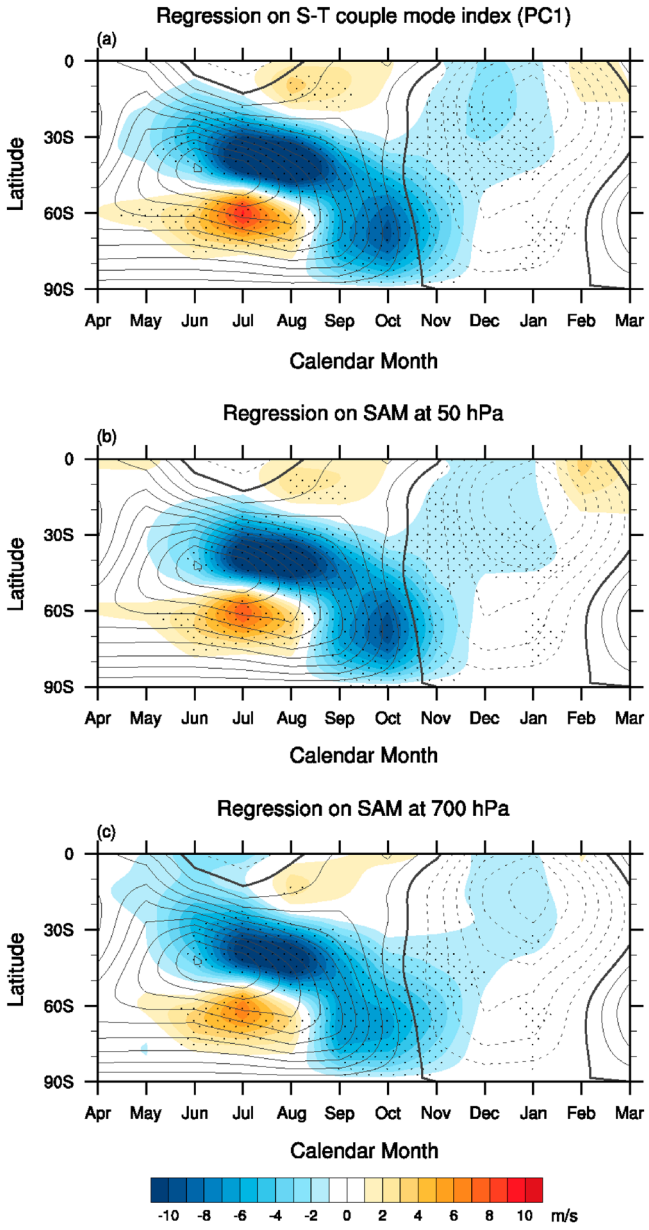


**Figure 6.** Regression of zonal mean-zonal wind anomalies at the 1-hPa level onto (a) PC1, onto (b) the October SAM at the 50-hPa level (supporting information Figure S3b) and onto (c) the October SAM at the 700-hPa level (Climate Prediction Center Antarctic Oscillation index; shading; interval is 1 m/s). The climatological zonal mean-zonal winds at the 1-hPa level is contoured (interval is 10 m/s; zero contour is thick and negative contours are dashed). Stippling indicates statistically significance of the regression at the 5% level, assessed with a two-tailed Student *t* test with 38 samples.

and moves poleward and downward through winter, weakens in spring, and finally breaks down in December through wave mean flow interactions (e.g., Hardiman et al., 2011; Hartmann et al., 1984; Hio & Yoden, 2005; Kodera & Kuroda, 2002). During the positive phase of the S-T coupled mode (i.e., weakening of the polar vortex), this poleward and downward progression of the westerly jet occurs earlier in the seasonal cycle, which leads to an earlier breakdown of the polar vortex (e.g., Byrne & Shepherd, 2018; Shiotani et al., 1993). The processes associated with an earlier than normal seasonal march are discussed in detail below.

The positive phase of the S-T coupled mode (i.e., polar vortex weakening) can be traced back to a meridional dipole anomaly in the zonal flow about the climatological mean stratopause jet in June, with anomalous westerlies on the poleward flank of the climatological mean jet and anomalous easterlies on the equatorward flank, thus depicting an anomalously poleward shift of the jet near the stratopause level (e.g., Hartmann et al., 1984; Shiotani et al., 1993). The westerly anomalies on the poleward flank of the stratospheric jet gradually weaken from July to September, by which time the EOF is dominated by easterly anomalies which move downward and poleward from August to November, in concert with the poleward and downward evolution of the climatological stratospheric westerly jet.

From October to December, the easterly anomalies propagate downward to the surface, projecting onto the negative polarity of the SAM during late spring to early summer, with easterly anomalies on the poleward side of the climatological mean tropospheric eddy-driven jet and westerly anomalies on the equatorward side. We will explore the relationship between the S-T coupling and the SAM in more detail in section 3.2.

The associated changes in the fluxes of wave activity, which drive the S-T coupled mode, are explored by regressing the anomalous Eliassen-Palm (E-P) flux and its divergence onto PC1 (Figure 5). Throughout the winter, the anomalies in the upper stratospheric zonal flow are driven by the anomalous upward and equatorward fluxes of wave activity at high latitudes (Figure 5 first and second rows). This pattern of E-P flux is consistent with the *focusing* and *preconditioning* of the stratospheric flow: The poleward shifted upper stratospheric westerly jet would allow waves with a greater range of phase velocities to higher levels (e.g., Andrews et al., 1987; Shepherd & McLandress, 2011) and also sets up a higher reflecting surface and a narrower meridional waveguide in the polar region, favoring more vertical propagation from below and more equatorward propagation in the higher levels of the stratosphere than usual (McIntyre, 1982; see also Limpasuvan et al., 2004; Randel, 1988; Shaw et al., 2010; Shiotani & Hirota, 1985; Figures 4 and 5).

From September the easterly forcing due to the convergence of anomalous upward wave fluxes overwhelms the westerly forcing exerted by that associated with the equatorward wave fluxes, and thus, easterly anomalies dominate in the SH extratropical stratosphere (Figures 4 and 5). In late spring, easterly flow in the stratosphere acts to inhibit anomalous upward propagation of wave activity from below and completes the anomalously early seasonal march of the polar vortex (e.g., Byrne & Shepherd, 2018; Shiotani et al., 1993). During October–December, the meridional dipole in tropospheric zonal wind anomalies associated with −ve SAM is driven by the meridional component of the E-P fluxes, consistent with variations in the tropospheric horizontal momentum flux (Hartmann & Lo, 1998; Figure 5).

**Table 1**
*Details of Climate Indices Used in This Study*

| Index | Description | Data |
|---|---|---|
| NINO3 | Sea surface temperature (SST) averaged over the NINO3 region (5°S to 5°N, 90°W to 150°W) | SST data of Hurrell et al. (2008) before 1982 and Reynolds et al. (2002) from 1982 |
| EMI (El Niño Modoki) | Difference of SST anomalies between the tropical central Pacific and the tropical eastern and western Pacific as follows (Ashok et al., 2007): EMI = $\overline{SST}$(165°E to 140°W, 10°S to 10°N) − 0.5 × $\overline{SST}$(110°W to 70°W, 15°S to 5°N) − 0.5 × $\overline{SST}$(125°E to 145°E,10°S to 20°N), where overbars indicate the area mean over the domain in the parentheses | SST data of Hurrell et al. (2008) before 1982 and Reynolds et al. (2002) from 1982 |
| CPC AAO (Climate Prediction Center Antarctic Oscillation) | Projection of the monthly anomalies of 700-hPa level geopotential height (GPH) anomalies poleward of 20°S onto the leading empirical orthogonal function pattern of the monthly 700-hPa level GPH anomalies of the period 1979–2000 (Thompson & Wallace, 2000) | Available online by National Oceanic and Atmospheric Administration Climate Prediction Center (http://www.cpc.ncep.noaa.gov/products/precip/CWlink/daily_ao_index/aao/aao.shtml) |

The E-P flux diagnostics reveal the wave-mean flow interactions that play an important role in variations in the polar vortex and its coupling with the surface circulation. However, many studies have argued that the dynamics of variations in the stratospheric vortex is not fully captured by zonally symmetric diagnostics such as those shown in Figure 5. For example, the vortex is often displaced from the pole and is disturbed by nonlinear processes such as wave-wave interaction, and these can be particularly important on intraseasonal timescales (e.g., Hio & Yoden, 2004; Hirota et al., 1990; Mechoso et al., 1988; O'Neill & Pope, 1988). A more detailed exploration of the role of wave-wave interactions in SH vortex variability in a separate study will be worthwhile.

### 3.2. Upper Stratospheric Origin of Springtime SAM

A key finding from the regression analysis presented above is that variations in the surface component of the SAM during austral spring and summer are seemingly linked not only to variations in the mid-stratosphere during the preceding 2 months, which has been shown in previous work (e.g., Byrne & Shepherd, 2018; Son et al., 2013; Thompson et al., 2005; Thompson & Solomon, 2002), but are also linked to variations in the flow near the stratopause level as early as June (e.g., Kuroda & Kodera, 1998; Shiotani et al., 1993).

The robustness of this linkage is supported by the regression maps shown in Figure 6. The top panel shows the regression of the zonal mean-zonal wind anomalies at the 1-hPa level onto the S-T coupled mode PC1 as a function of latitude and month (Figure 6a). Also shown is the climatological zonal mean-zonal wind at 1 hPa. Figure 6a highlights the development of the meridional dipole of zonal wind anomalies about the climatological stratospheric jet in the midlatitudes as early as June, the poleward progression of the anomalies through the winter and spring season, and a monopole wind anomaly from September onward, which was discussed with Figure 4.

The middle panel (Figure 6b) displays the regression of the zonal mean-zonal wind anomalies at the 1-hPa level onto the October SAM index at the 50-hPa level. The SAM index at 50 hPa is defined here as the leading principal component of October mean geopotential height variability at the 50-hPa level over 30–90°S (supporting information Figure S3). The results in Figure 6b are nearly identical to those in Figure 6a, which highlights both the usefulness of the height-time EOF analysis for capturing variations in the strength of the stratospheric polar vortex and the robustness of the connection between variations in the stratospheric vortex at the 50-hPa level during October and those in the upper stratospheric flow in early winter. Note that the 50-hPa SAM index is significantly correlated with the lower tropospheric SAM at the 700-hPa level in October ($r \sim 0.66$; the 700-hPa SAM index is the October time series of the Climate Prediction Center Antarctic Oscillation index [AAO]; see Table 1 for details of Climate Prediction Center AAO).

The bottom panel of Figure 6 shows analogous results but for the regression of the zonal mean zonal flow at the 1-hPa level onto the variations in the SAM at the 700-hPa level during October (Figure 6c). Despite the extraordinary differences in atmospheric mass between the 1- and 700-hPa levels, variations in the tropospheric SAM during the spring months are robustly linked to variations in the flow well into the upper stratosphere as early as June.

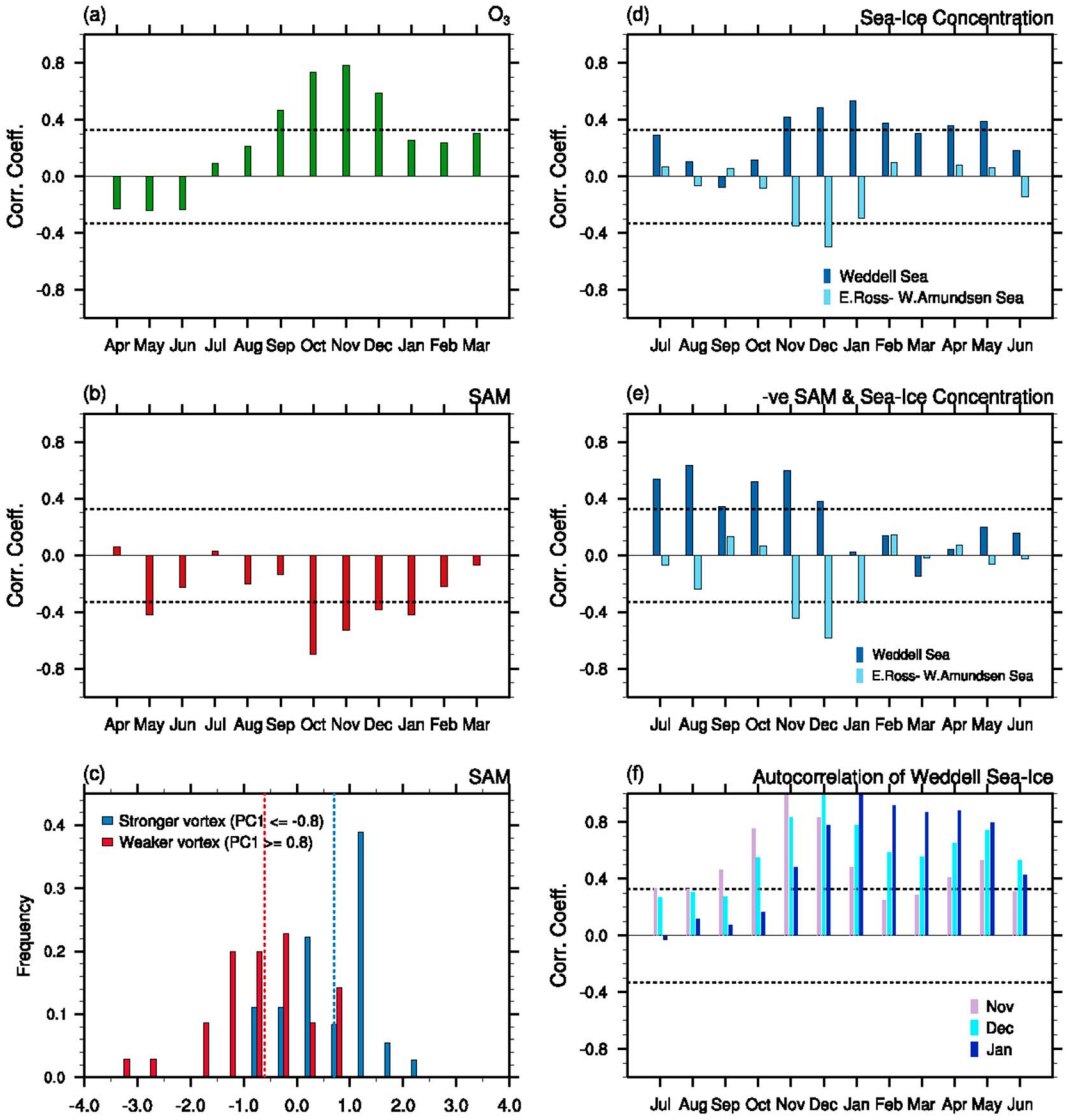


**Figure 7.** (left column) Correlation of the S-T coupled mode index (PC1) with (a) monthly total column ozone averaged over 60–90°S and (b) monthly SAM (CPC AAO). The total column ozone data are from the KNMI multisensor reanalysis (van Der et al., 2010) and available at http://www.temis.nl/protocols/o3field/o3mean_msr.php. (c) Frequency distribution of monthly SAM index values during October to January for strong positive (PC1 $\geq 0.8\sigma$) and negative (PC1 $\leq -0.8\sigma$) polarities of the S-T coupled mode. (right column) (d) Correlation of PC1 with monthly sea ice concentrations over the Weddell Sea (60–90°S, 300–345°E; dark blue bars) and the eastern Ross Sea to the western Amundsen Sea (50–65°S, 190–240°E; light blue bars), (e) same as (d) but the sea ice concentration is correlated with negative SAM with 1-month lag, and (f) autocorrelation of the Weddell Sea sea ice concentration of November (purple bars), December (light blue bars), and January (dark blue bars). The abscissa of (d) and (e) indicates the months of sea ice. Sea ice concentration data are from the National Snow and Ice Data Center and available at https://nsidc.org/data/seaice. The ozone, SAM and sea ice concentration time series used here were deseasonalized and detrended before the correlation calculation. The horizontal dash lines indicate the statistically significant correlation at the 5% level, assessed with a two-tailed Student *t* test given 38 samples.

The implied predictability of the lower tropospheric SAM during spring that derives from anomalies in the upper stratospheric condition during early winter is explored further by developing a *leave-one-out* cross-validated lagged-regression prediction between the 1-hPa level zonal mean-zonal winds at 65°S during June and July and the SAM index at 700-hPa level during October for the period 1979–2016 (e.g., Seviour et al., 2014). The correlation skill for predicting the October SAM index using the upper stratospheric zonal mean-zonal winds during June and July is 0.29 (significant at $p$ = 10%) and 0.35 (significant at $p$ = 5%),

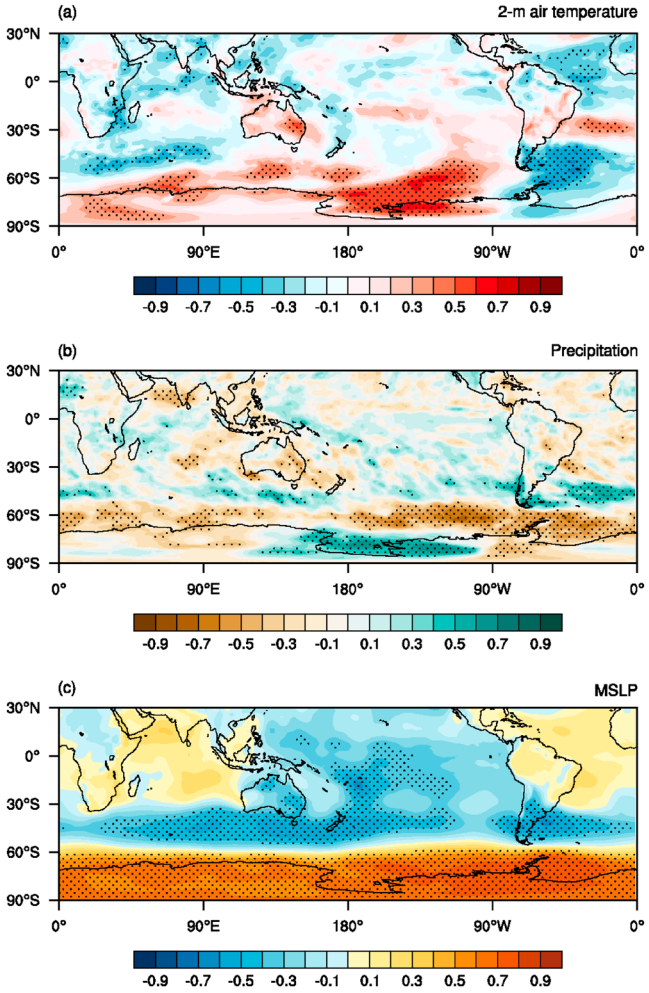


**Figure 8.** Correlation of the S-T coupled mode PC1 with October–January mean (a) 2-m air temperature, (b) precipitation, and (c) mean sea level pressure (MSLP) anomalies. Before the correlation calculation, a linear trend and the influence of eastern Pacific and central Pacific El Niño–Southern Oscillation were removed from the temperature, precipitation, and MSLP data by regressing out the relationship with time and the NINO3 and El Niño Modoki indices using multiple linear regression (details of the NINO3 and El Niño Modoki indices can be found in Table 1). Stippling indicates statistically significant correlation at the 5% level, assessed by a two-tailed Student *t* test with 38 samples.

respectively. The non-cross-validated correlations are 0.44 and 0.43. The cross-validated correlation values are comparable to the springtime SAM prediction skill in the lower troposphere demonstrated by Seviour et al. (2014) who used the Antarctic polar cap geopotential height anomalies at the 10-hPa level on 1 August as a predictor (their Figure 7b). Byrne and Shepherd (2018) also showed a moderate but statistically significant (non-cross-validated) correlation between the Antarctic polar cap geopotential height anomalies at the 30-hPa level during August and the surface SAM of October to November ($r$ = 0.36; their Figure 14a). Our results suggest that predictability of the lower tropospheric SAM during spring can be extended up to 2 months earlier than the time proposed in Seviour et al. (2014) and Byrne and Shepherd (2018) by using anomalous conditions from a higher level of the stratosphere (e.g., 1 hPa). This extension to earlier lead times by moving higher up in the stratosphere makes sense given that the anomalous polar vortex signal detected at the 10- and 30-hPa levels during August can be traced upward to possibly the lower mesosphere-upper stratosphere level 2–3 months earlier (Figure 4; see also Hartmann et al., 1984; Hardiman et al., 2011; Kuroda & Kodera, 1998; Shiotani et al., 1993).

## 4. Impacts of the S-T Coupled Mode

The association of the S-T coupled mode with the SAM, both at the surface and aloft, implies that the S-T coupled mode is linked to variations in a variety of phenomena throughout the troposphere and stratosphere. For instance, the S-T coupled mode is closely linked to variations in Antarctic polar ozone concentration ($O_3$), as evidenced by the strong correlations between detrended values of monthly mean polar cap $O_3$ with the S-T coupled mode PC1 during austral spring to early summer (Figure 7a). As summarized by Stolarski et al. (2005) and Seviour et al. (2014; and also observed during the SH SSW of 2002), weakenings of the Antarctic polar vortex are associated with higher concentrations of $O_3$ in the lower stratosphere and vice versa.

As suggested in Figures 4 and 6, the S-T coupled mode PC1is also significantly correlated with the tropospheric component of the SAM from October to January (Figure 7b). The histogram of monthly SAM values at the 700-hPa level during October–January is displayed in Figure 7c, stratified for strong positive and negative values of PC1. Positive values of the S-T coupled mode are strongly linked to negative values of the SAM and vice versa. The difference in the means of the two distributions is statistically significant at the 99.9% confidence level, with an especially apparent impact on the frequency of occurrence of extreme SAM excursions.

The strong relationship between the S-T coupled mode and the lower tropospheric SAM implies a similarly strong relationship with other aspects of climate that are sensitive to the SAM. For example, the positive polarity of the S-T coupled mode is associated with lower than normal sea ice concentrations in the eastern Ross Sea-western Amundsen Sea and higher than normal sea ice concentrations over the Weddell Sea, which are similar to the respective sea ice responses to the negative polarity of the SAM (Lefebvre et al., 2004; Simpkins et al., 2012; Figures 7d and 7e). However, it is interesting to note that the linkages between the Weddell Sea sea ice anomalies and the tropospheric SAM are stronger in the winter-spring seasons (Figure 7e), whereas the linkages to the S-T coupled mode persist from late spring to the following autumn (Figure 7d). The difference between Figures 7d and 7e seems to derive from the fact that the S-T coupled mode is only linked to the surface component of the SAM during spring to summer months when the Weddell Sea sea ice has strong persistence for the following several months (Figure 7f). For instance,

Figure 7f indicates that the Weddell Sea sea ice state in December and January tends to persist through May; therefore, the impact of the S-T coupling on the Weddell Sea sea ice during December to January is carried through to the following autumn. In contrast, the impact of the S-T coupling on the sea ice over the eastern Ross Sea-western Amundsen Sea over 50–65°S is limited to November to January because the South Pacific sea ice substantially retreats poleward in summer months (e.g., Simpkins et al., 2012; the autocorrelations of the sea ice over the eastern Ross Sea-western Amundsen Sea over 50–65°S of November to January all drop to near zero by February; supporting information Figure S4).

The S-T coupled mode also has impacts on regional surface climate variations throughout the SH subpolar regions via its association with the SAM. The correlation of PC1 with October–January mean 2-m air temperature, rainfall, and mean sea level pressure (MSLP) is displayed in Figure 8. The signature of −ve SAM is seen throughout the SH, including the equatorward shift of rainfall in the high latitude storm track; variations in MSLP throughout the mid- and high latitudes; drier and warm conditions over subtropical Australia; cooler temperatures over south eastern Africa; and more rainfall over the southern end of South America (Bandoro et al., 2014; Garreaud et al., 2013; Gillett et al., 2006; Hendon et al., 2007; Silvestri & Vera, 2003; Son et al., 2013).

## 5. Concluding Remarks

In this study, we have objectively identified the leading mode of seasonally locked, SH S-T vertical coupling by applying height-time domain EOF analysis to monthly mean, zonal mean-zonal winds in the Antarctic circumpolar region of 55–65°S. Time domain EOF analysis has previously been used to capture SH polar vortex variability that is strongly tied to the seasonality of the vortex breakdown (e.g., Byrne & Shepherd, 2018; Hio & Yoden, 2005; Kuroda & Kodera, 1998; Taguchi & Yoden, 2002). Our results build on these previous studies by tracking the anomalous preceding conditions higher and earlier in the stratosphere. The key novel result is that variations in the tropospheric circulation during spring and summer are significantly linked to variations in the extratropical jet as high as the stratopause and as early as June.

The leading EOF pattern, which we refer to as the S-T coupled mode, is characterized by near-stratopause zonal mean-zonal wind anomalies over the circumpolar region in early winter that then change sign in early spring, peak in amplitude in the upper-middle stratosphere in October, and extend downward to the surface from October through January. As Shiotani et al. (1993) showed, the positive to negative sign change of $U_{55–65°S}$ from winter to early spring depicted by the EOF pattern indicates earlier seasonal progression of the polar vortex. The S-T coupled mode accounts for 42% of the vertical-temporal variance of the Antarctic circumpolar zonal mean-zonal winds that is phase locked to the seasonal cycle.

The dynamical evolution of the S-T coupled mode is characterized by a meridional dipole in the subtropical zonal flow at the stratopause level in June and variations in the strength of the extratropical vortex during the winter to spring seasons. Anomalous weakening of the polar vortex (i.e., earlier seasonal march) in the SH during spring is marked by a poleward shift of the upper stratospheric westerly jet during June, with anomalous westerlies on the poleward flank of the climatological jet centered ~40°S and anomalous easterlies on the equatorward flank. The poleward shifted upper stratospheric jet (i.e., increased speed of background zonal mean flow) allows waves with a various range of phase velocities to propagate to higher levels (e.g., Andrews et al., 1987; Shepherd & McLandress, 2011) and sets up a higher reflecting surface and a narrower meridional waveguide in the polar region, which favors more vertical propagation from the troposphere and more equatorward propagation in the higher levels of the stratosphere than usual (Limpasuvan et al., 2004; McIntyre, 1982; Randel, 1988; Shaw et al., 2010; Shiotani & Hirota, 1985). As a result, the meridional dipole of zonal wind anomalies strengthens and shifts poleward and downward through winter in conjunction with the poleward and downward evolution of the polar night jet. By the end of winter, the easterly forcing due to convergence of anomalous upward wave fluxes is larger than the westerly forcing exerted by the divergence of the equatorward wave fluxes, and thus the westerly anomalies on the poleward flank of the jet disappear, while the easterly anomalies on the equatorward flank of the jet continue to strengthen, move poleward, and descend, thus resulting in an anomalously weak vortex. From October–December, the easterly anomalies extend downward to the surface in association with changes in the tropospheric momentum fluxes. In the troposphere during spring and summer, the positive polarity of the S-T coupled mode projects onto the negative polarity of the SAM and is thus linked to a range of surface climate impacts.

We have shown that variations in the surface component of the SAM during late spring and summer are linked not only to variations in the stratosphere during the preceding ~1–2 months (as has been shown in many previous studies) but also to variations near the stratopause level as early as June as well. We have thus shown that the state of the upper stratospheric flow during the early winter months is a potential source of predictability for variations in the tropospheric SAM and its associated surface climate impacts during spring–summer. Since the S-T coupled mode is not significantly linked to ENSO (supporting information Figure S2), the predictability inferred here is in addition to that associated with ENSO variability (e.g., L'Heureux & Thompson, 2006; Lim et al., 2013; Lim & Hendon, 2015a; Zhou & Yu, 2004). Improved resolution of the stratosphere has previously been shown to result in improved prediction of tropospheric variations in the SAM (e.g., Roff et al., 2011). Ongoing research using a high-top model with a well-resolved stratosphere will address the predictability of the S-T coupled mode, its sensitivity to stratospheric initial conditions, and its impact on long-lead prediction of the SAM.

**Acknowledgments**

This research was supported in part by Meat & Livestock Australia (MLA) and the Australian Department of Agriculture and Water Resources. David W. J. Thompson is supported by the U.S. National Science Foundation Climate Dynamics Program. The authors are very much grateful for constructive feedback and comments provided by three anonymous reviewers and Andrew Dowdy and Matt Tully at the Australian Bureau of Meteorology. This research was undertaken on the NCI National Facility in Canberra, Australia, which is supported by the Australian Commonwealth Government. The NCAR Command Language (NCL; http://www.ncl.ucar.edu) version 6.4.0 was used for data analysis and visualization of the results. We also acknowledge NCAR/UCAR, NOAA, NSIDC, the UK Met Office, ECMWF, and KNMI for producing and providing Hurrell et al. (2008) SST analysis, Reynolds OI v2 SST analysis, sea ice data, HadISST analysis, ERA-Interim reanalysis, and ozone data.

## References

Andrews, D. G., Holton, J. R., & Leovy, C. B. (1987). *Middle atmosphere dynamics*. London: Academic Press, Inc.

Arblaster, J. M., Lim, E.-P., Hendon, H. H., Trewin, B. C., Wheeler, M. C., Liu, G., & Braganza, K. (2014). Understanding Australia's hottest September on record. *Bulletin of the American Meteorological Society*, *95*(9), S37–S41.

Ashok, K., Behera, S. K., Rao, S. A., Weng, H., & Yamagata, T. (2007). El Niño Modoki and its possible teleconnection. *Journal of Geophysical Research*, *112*, C11007. https://doi.org/10.1029/2006JC003798

Baldwin, M. P., & Dunkerton, T. J. (1999). Propagation of the Arctic Oscillation from the stratosphere to the troposphere. *Journal of Geophysical Research*, *104*(D24), 30,937–30,946. https://doi.org/10.1029/1999JD900445

Baldwin, M. P., & Dunkerton, T. J. (2001). Stratospheric harbingers of anomalous weather regimes. *Science*, *294*(5542), 581–584. https://doi.org/10.1126/science.1063315

Baldwin, M. P., Stephenson, D. B., Thompson, D. W. J., Dunkerton, T. J., Charlton, A. J., & O'Neill, A. (2003). Stratospheric memory and skill of extended-range weather forecasts. *Science (New York, N.Y.)*, *301*(5633), 636–640. https://doi.org/10.1126/science.1087143

Bandoro, J., Solomon, S., Donohoe, A., Thompson, D. W. J., & Santer, B. D. (2014). Influences of the Antarctic ozone hole on Southern Hemispheric summer climate change. *Journal of Climate*, *27*(16), 6245–6264. https://doi.org/10.1175/JCLI-D-13-00698.1

Black, R. X., & McDaniel, B. A. (2007). Interannual variability in the Southern Hemisphere circulation organized by stratospheric final warming events. *Journal of the Atmospheric Sciences*, *64*(8), 2968–2974. https://doi.org/10.1175/JAS3979.1

Butler, A. H., Seidel, D. J., Hardiman, S. C., Butchart, N., Birner, T., & Match, A. (2015). Defining sudden stratospheric warmings. *Bulletin of the American Meteorological Society*, *96*(11), 1913–1928. https://doi.org/10.1175/BAMS-D-13-00173.1

Byrne, N. J., & Shepherd, T. G. (2018). Seasonal persistence of circulation anomalies in the Southern Hemisphere stratosphere and its implications for the troposphere. *Journal of Climate*, *31*(9), 3467–3483. https://doi.org/10.1175/JCLI-D-17-0557.1

Byrne, N. J., Shepherd, T. G., Woollings, T., & Plumb, R. A. (2017). Nonstationarity in Southern Hemisphere climate variability associated with the seasonal breakdown of the stratospheric polar vortex. *Journal of Climate*, *30*(18), 7125–7139. https://doi.org/10.1175/JCLI-D-17-0097.1

Charlton, A. J., O'Neill, A., Stephenson, D. B., Lahoz, W. A., & Baldwin, M. P. (2003). Can knowledge of the state of the stratosphere be used to improve statistical forecasts of the troposphere? *Quarterly Journal of the Royal Meteorological Society*, *129*(595 PART B), 3205–3224. https://doi.org/10.1256/qj.02.232

Dee, D., Uppala, S., Simmons, A., Berrisford, P., Poli, P., Kobayashi, S., et al. (2011). The ERA-Interim reanalysis: Configuration and performance of the data assimilation system. *Quaterly Journal of the Royal Meteorological Society*, *137*(656), 553–597. https://doi.org/10.1002/qj.828

Dowdy, A. J., Vincent, R. A., Tsutsumi, M., Igarashi, K., Murayama, Y., Singer, W., Murphy, D. J., et al. (2007). Polar mesosphere and lower thermosphere dynamics: 2. Response to sudden stratospheric warmings. *Journal of Geophysical Research*, *112*, 1–14. https://doi.org/10.1029/2006JD008127

Garreaud, R., Lopez, P., Minvielle, M., & Rojas, M. (2013). Large-scale control on the Patagonian climate. *Journal of Climate*, *26*(1), 215–230. https://doi.org/10.1175/JCLI-D-12-00001.1

Gillett, N. P., Kell, T. D., & Jones, P. D. (2006). Regional climate impacts of the Southern Annular Mode. *Geophysical Research Letters*, *33*, L23704. https://doi.org/10.1029/2006GL027721

Graversen, R. G., & Christiansen, B. (2003). Downward propagation from the stratosphere to the troposphere: A comparison of the two hemispheres. *Journal of Geophysical Research*, *108*(D24), 4780. https://doi.org/10.1029/2003JD004077

Gupta, A. S., & England, M. H. (2006). Coupled ocean-atmosphere-ice response to variations in the southern annular mode. *Journal of Climate*, *19*(18), 4457–4486. https://doi.org/10.1175/JCLI3843.1

Hall, A., & Visbeck, M. (2002). Synchronous variability in the Southern Hemisphere atmosphere, sea ice, and ocean resulting from the annular mode. *Journal of Climate*, *15*(21), 3043–3057. https://doi.org/10.1175/1520-0442(2002)015<3043:SVITSH>2.0.CO;2

Hardiman, S. C., Butchart, N., Charlton-Perez, A. J., Shaw, T. A., Akiyoshi, H., Baumgaertner, A., Bekki, S., et al. (2011). Improved predictability of the troposphere using stratospheric final warmings. *Journal of Geophysical Research*, *116*, D18113. https://doi.org/10.1029/2011JD015914

Hartmann, D. L., & Lo, F. (1998). Wave-driven zonal flow vacillation in the Southern Hemisphere. *Journal of the Atmospheric Sciences*, *55*(8), 1303–1315. https://doi.org/10.1175/1520-0469(1998)055<1303:WDZFVI>2.0.CO;2

Hartmann, D. L., Mechoso, C. R., & Yamazaki, K. (1984). Observations of wave-mean flow interaction in the Southern Hemisphere. *Journal of the Atmospheric Sciences*, *41*(3), 351–362. https://doi.org/10.1175/1520-0469(1984)041<0351:OOWMFI>2.0.CO;2

Hendon, H. H., Lim, E.-P., & Nguyen, H. (2014). Seasonal variations of subtropical precipitation associated with the Southern Annular Mode. *Journal of Climate*, *27*(9), 3446–3460. https://doi.org/10.1175/JCLI-D-13-00550.1

Hendon, H. H., Thompson, D. W. J., & Wheeler, M. C. (2007). Australian rainfall and surface temperature variations associated with the Southern Hemisphere annular mode. *Journal of Climate*, *20*(11), 2452–2467. https://doi.org/10.1175/JCLI4134.1

Hio, Y., & Yoden, S. (2004). Quasi-periodic variations of the polar vortex in the Southern Hemisphere stratosphere due to wave–wave interaction. *Journal of the Atmospheric Sciences*, *61*(21), 2510–2527. https://doi.org/10.1175/JAS3257.1

Hio, Y., & Yoden, S. (2005). Interannual variations of the seasonal march in the Southern Hemisphere stratosphere for 1979–2002 and characterization of the unprecedented year 2002. *Journal of the Atmospheric Sciences*, *62*(3), 567–580. https://doi.org/10.1175/JAS-3333.1

Hirano, S., Kohma, M., & Sato, K. (2016). A three-dimensional analysis on therole of atmospheric waves in theclimatology and interannual variabilityof stratosphericfinal warming in the Southern Hemisphere. *Journal of Geophysical Research: Atmospheres*, *121*, 8429–8443. https://doi.org/10.1002/2015JD024481

Hirota, I., Kuroi, K., & Shiotani, M. (1990). Midwinter warmings in the southern hemisphere stratosphere in 1988. *Quarterly Journal of the Royal Meteorological Society*, *116*(494), 929–941. https://doi.org/10.1002/qj.49711649407

Hurrell, J. W., Hack, J. J., Shea, D., Caron, J. M., & Rosinski, J. (2008). A new sea surface temperature and sea ice boundary dataset for the community atmosphere model. *Journal of Climate*, *21*(19), 5145–5153. https://doi.org/10.1175/2008JCLI2292.1

Hurwitz, M. M., Calvo, N., Garfinkel, C. I., Butler, A. H., Ineson, S., Cagnazzo, C., Manzini, E., et al. (2014). Extra-tropical atmospheric response to ENSO in the CMIP5 models. *Climate Dynamics*, *43*(12), 3367–3376. https://doi.org/10.1007/s00382-014-2110-z

Hurwitz, M. M., Newman, P. A., Oman, L. D., & Molod, A. M. (2011). Response of the Antarctic stratosphere to two types of El Niño events. *Journal of the Atmospheric Sciences*, *68*(4), 812–822. https://doi.org/10.1175/2011JAS3606.1

Kang, S. M., Polvani, L. M., Fyfe, J. C., & Sigmond, M. (2011). Impact of polar ozone depletion on subtropical precipitation. *Science*, *332*(6032), 951–954. https://doi.org/10.1126/science.1202131

Karoly, D. J. (1990). The role of transient eddies in low-frequency zonal variations of the southern hemisphere circulation. *Tellus A*, *42*(1), 41–50. https://doi.org/10.1034/j.1600-0870.1990.00005.x

Kidson, J. W. (1988). Indices of the Southern Hemisphere zonal wind. *Journal of Climate*, *1*(2), 183–194. https://doi.org/10.1175/1520-0442(1988)001<0183:IOTSHZ>2.0.CO;2

Kidston, J., Scaife, A. A., Hardiman, S. C., Mitchell, D. M., Butchart, N., Baldwin, M. P., & Gray, L. J. (2015). Stratospheric influence on tropospheric jet streams, storm tracks and surface weather. *Nature Geoscience*, *8*(6), 433–440. https://doi.org/10.1038/ngeo2424

Kobayashi, S., Ota, Y., Harada, Y., Ebita, A., Moriya, M., Onoda, H., et al. (2015). The JRA-55 reanalysis: General specifications and basic characteristics. *Journal of the Meteorological Society of Japan Ser. II*, *93*(1), 5–48. https://doi.org/10.2151/jmsj.2015-001

Kodera, K., & Kuroda, Y. (2002). Dynamical response to the solar cycle. *Journal of Geophysical Research*, *107*(D24), 4749. https://doi.org/10.1029/2002JD002224

Kuroda, Y., & Kodera, K. (1998). Interannual variability in the troposphere and stratosphere of the southern hemisphere winter. *Journal of Geophysical Research*, *103*(D12), 13,787–13,799. https://doi.org/10.1029/98JD01042

Lefebvre, W., Goosse, H., Timmermann, R., & Fichefet, T. (2004). Influence of the Southern Annular Mode on the sea ice-ocean system. *Journal of Geophysical Research*, *109*, C09005. https://doi.org/10.1029/2004JC002403

L'Heureux, M. L., & Thompson, D. W. J. (2006). Observed relationships between the El Niño–Southern Oscillation and the extratropical zonal-mean circulation. *Journal of Climate*, *19*(2), 276–287. https://doi.org/10.1175/JCLI3617.1

Lim, E., Hendon, H. H., Arblaster, J. M., Delage, F., & Nguyen, H. (2016). The impact of the Southern Annular Mode on future changes in Southern Hemisphere rainfall. *Geophysical Research Letters*, *43*, 7160–7167. https://doi.org/10.1002/2016GL069453.Received

Lim, E. P., & Hendon, H. H. (2015a). Understanding and predicting the strong Southern Annular Mode and its impact on the record wet east Australian spring 2010. *Climate Dynamics*, *44*(9–10), 2807–2824. https://doi.org/10.1007/s00382-014-2400-5

Lim, E.-P., & Hendon, H. H. (2015b). Understanding the contrast of Australian springtime rainfall of 1997 and 2002 in the frame of two flavors of El Niño. *Journal of Climate*, *28*(7), 2804–2822. https://doi.org/10.1175/JCLI-D-14-00582.1

Lim, E.-P., Hendon, H. H., & Rashid, H. (2013). Seasonal predictability of the Southern Annular Mode due to its association with ENSO. *Journal of Climate*, *26*(20), 8037–8054. https://doi.org/10.1175/JCLI-D-13-00006.1

Limpasuvan, V., Hartmann, D. L., Thompson, D. W. J., Jeev, K., & Yung, Y. L. (2005). Stratosphere-troposphere evolution during polar vortex intensification. *Journal of Geophysical Research*, *110*, D24101. https://doi.org/10.1029/2005JD006302

Limpasuvan, V., Thompson, D. W. J., & Hartmann, D. L. (2004). On the life cycle of Northern Hemisphere stratospheric sudden warming. *Journal of Climate*, *17*(13), 2584–2596. https://doi.org/10.1175/1520-0442(2004)017<2584:TLCOTN>2.0.CO;2

Marshall, G. J., Thompson, D. W. J., & van den Broeke, M. R. (2017). The signature of Southern Hemisphere atmospheric circulation patterns in Antarctic precipitation. *Geophysical Research Letters*, *44*, 11,580–11,589. https://doi.org/10.1002/2017GL075998

McIntyre, M. E. (1982). How well do we understand the dynamics of stratospheric warmings? *Journal of the Meteorological Society of Japan*, *60*(1), 37–65.

Mechoso, C. R., O'Neill, A., Pope, V. D., & Farrara, J. D. (1988). A study of the stratospheric final warming of 1982 in the Southern Hemisphere. *Quarterly Journal of the Royal Meteorological Society*, *114*(484), 1365–1384. https://doi.org/10.1002/qj.49711448402

Menary, M. B., & Scaife, A. A. (2014). Naturally forced multidecadal variability of the Atlantic meridional overturning circulation. *Climate Dynamics*, *42*(5–6), 1347–1362. https://doi.org/10.1007/s00382-013-2028-x

Newman, P., & Nash, E. (2005). The unusual Southern Hemisphere stratosphere winter of 2002. *Journal of the Atmospheric Sciences*, *62*(3), 614–628. https://doi.org/10.1175/JAS-3323.1

North, G. R., Bell, T. L., Cahalan, R. F., & Moeng, F. J. (1982). Sampling errors in the estimation of empirical orthogonal functions. *Monthly Weather Review*, *110*(7), 699–706. https://doi.org/10.1175/1520-0493(1982)110<0699:SEITEO>2.0.CO;2

O'Neill, A., & Pope, V. D. (1988). Simulations of linear and nonlinear disturbances in the stratosphere. *Quarterly Journal of the Royal Meteorological Society*, *114*(482), 1063–1110. https://doi.org/10.1002/qj.49711448210

Peixoto, J. P., & Oort, A. H. (1992). *Physics of climate* (1st ed.). AIP-Press.

Randel, W. J. (1988). The seasonal evolution of planetary-waves in the Southern-Hemisphere stratosphere and troposphere. *Quarterly Journal of the Royal Meteorological Society*, *114*(484), 1385–1409. https://doi.org/10.1002/qj.49711448403

Reason, C. J. C., & Rouault, M. (2005). Links between the Antarctic Oscillation and winter rainfall over western South Africa. *Geophysical Research Letters*, *32*, L07705. https://doi.org/10.1029/2005GL022419

Reichler, T., Kim, J., Manzini, E., & Kröger, J. (2012). A stratospheric connection to Atlantic climate variability. *Nature Geoscience*, *5*(11), 783–787. https://doi.org/10.1038/ngeo1586

Reynolds, R. W., Rayner, N. A., Smith, T. M., Stokes, D. C., & Wang, W. (2002). An improved in situ and satellite SST analysis for climate. *Journal of Climate*, *15*(13), 1609–1625. https://doi.org/10.1175/1520-0442(2002)015<1609:AIISAS>2.0.CO;2

Roff, G., Thompson, D. W. J., & Hendon, H. (2011). Does increasing model stratospheric resolution improve extended-range forecast skill? *Geophysical Research Letters*, *38*, L05809. https://doi.org/10.1029/2010GL046515

Seager, R., Harnik, N., Kushnir, Y., Robinson, W. A., & Miller, J. A. (2003). Mechanisms of hemispherically symmetric climate variability. *Journal of Climate*, *16*(18), 2960–2978. https://doi.org/10.1175/1520-0442(2003)016<2960:MOHSCV>2.0.CO;2

Seviour, W. J. M., Hardiman, S. C., Gray, L. J., Butchart, N., MacLachlan, C., & Scaife, A. A. (2014). Skillful seasonal prediction of the Southern Annular Mode and Antarctic ozone. *Journal of Climate*, *27*(19), 7462–7474. https://doi.org/10.1175/JCLI-D-14-00264.1

Shaw, T. A., Perlwitz, J., & Harnik, N. (2010). Downward wave coupling between the stratosphere and troposphere: The importance of meridional wave guiding and comparison with zonal-mean coupling. *Journal of Climate*, *23*(23), 6365–6381. https://doi.org/10.1175/2010JCLI3804.1

Shepherd, T. G., & McLandress, C. (2011). A robust mechanism for strengthening of the Brewer–Dobson circulation in response to climate change: Critical-layer control of subtropical wave breaking. *Journal of the Atmospheric Sciences*, *68*(4), 784–797. https://doi.org/10.1175/2010JAS3608.1

Shiotani, M., & Hirota, I. (1985). Planetary wave-mean flow interaction in the stratosphere: A comparison between northern and southern hemispheres. *The Quarterly Journal of the Royal Meteorological Society*, *111*(468), 309–334. https://doi.org/10.1002/qj.49711146404

Shiotani, M., Shimoda, N., & Hirota, I. (1993). Interannual variability of the stratospheric circulation in the Southern-Hemisphere. *Quarterly Journal of the Royal Meteorological Society*, *119*(511), 531–546. https://doi.org/10.1002/qj.49711951110

Sigmond, M., Scinocca, J. F., Kharin, V. V., & Shepherd, T. G. (2013). Enhanced seasonal forecast skill following stratospheric sudden warmings. *Nature Geoscience*, *6*(2), 98–102. https://doi.org/10.1038/ngeo1698

Silvestri, G. E., & Vera, C. S. (2003). Antarctic Oscillation signal on precipitation anomalies over southeastern South America. *Geophysical Research Letters*, *30*(21), 2115. https://doi.org/10.1029/2003GL018277

Simpkins, G. R., Ciasto, L. M., Thompson, D. W. J., & England, M. H. (2012). Seasonal relationships between large-scale climate variability and Antarctic sea ice concentration. *Journal of Climate*, *25*(16), 5451–5469. https://doi.org/10.1175/JCLI-D-11-00367.1

Solomon, S., Ivy, D. J., Kinnison, D., Mills, M. J., Iii, R. R. N., & Schmidt, A. (2016). Emergence of healing in the Antarctic ozone layer. *353*(6296), 269–274. https://doi.org/10.1126/science.aae0061

Son, S. W., Purich, A., Hendon, H. H., Kim, B. M., & Polvani, L. M. (2013). Improved seasonal forecast using ozone hole variability? Supplementary Info. *Geophysical Research Letters*, *40*, 6231–6235. https://doi.org/10.1002/2013GL057731

Stolarski, R. S., McPeters, R. D., & Newman, P. a. (2005). The ozone hole of 2002 as measured by TOMS. *Journal of the Atmospheric Sciences*, *62*(3), 716–720. https://doi.org/10.1175/JAS-3338.1

Taguchi, M., & Yoden, S. (2002). Internal interannual variability of the troposphere–stratosphere coupled system in a simple global circulation model. Part I: Parameter Sweep Experiment. *Journal of the Atmospheric Sciences*, *59*(21), 3021–3036. https://doi.org/10.1175/1520-0469(2002)059<3021:IIVOTT>2.0.CO;2

Thompson, D. W. J., Baldwin, M. P., & Solomon, S. (2005). Stratosphere–troposphere coupling in the Southern Hemisphere. *Journal of the Atmospheric Sciences*, *62*(3), 708–715. https://doi.org/10.1175/JAS-3321.1

Thompson, D. W. J., & Solomon, S. (2002). Interpretation of recent Southern Hemisphere climate change. *Science*, *296*(5569), 895–899. https://doi.org/10.1126/science.1069270

Thompson, D. W. J., & Wallace, J. M. (2000). Annular mode in the extratropical circulation. Part I: Month-to-month variability. *Journal of Climate*, *13*(5), 1000–1016. https://doi.org/10.1175/1520-0442(2000)013<1000:AMITEC>2.0.CO;2

van Der, A. R. J., Allaart, M. A. F., & Eskes, H. J. (2010). Multi sensor reanalysis of total ozone. *Atmospheric Chemistry and Physics*, *10*(22), 11277–11294. https://doi.org/10.5194/acp-10-11277-2010

Waugh, D. W., Randel, W. J., Pawson, S., Newman, P. A., & Nash, E. R. (1999). Persistence of the lower stratospheric polar vortices. *Journal of Geophysical Research*, *104*(D22), 27191–27201. https://doi.org/10.1029/1999JD900795

World Meteorological Organization (2003). WMO statement on the status of the global climate in 2002. World Meteorological Organization. Retrieved from http://www.wmo.int/pages/mediacentre/press_releases/documents/WMO_1108_EN_web_000.pdf

Zhou, T. J., & Yu, R. C. (2004). Sea-surface temperature induced variability of the Southern Annular Mode in an atmospheric general circulation model. *Geophysical Research Letters*, *31*, L24206. https://doi.org/10.1029/2004GL021473